AFRL-ML-WP-TR-2006-4112

DEVELOPMENT OF MULTIAXIAL FATIGUE DAMAGE ASSESSMENT METHODS CONSIDERING HIGH CYCLE FATIGUE (HCF)/LOW CYCLE FATIGUE (LCF) INTERACTIONS

Dr. Alan R. Kallmeyer

North Dakota State University
Department of Mechanical Engineering and Applied Mechanics
1301 12th Avenue N
Fargo, ND 58105-3400

Dr. Peter Kurath

University of Illinois – Urbana-Champaign
Department of Mechanical Engineering
Urbana, IL 61801

APRIL 2006

Final Report for 18 February 2004 – 31 March 2006

MATERIALS AND MANUFACTURING DIRECTORATE
AIR FORCE RESEARCH LABORATORY
AIR FORCE MATERIEL COMMAND
WRIGHT-PATTERSON AIR FORCE BASE, OH 45433-7750

NOTICE

This report was cleared for public release by the Air Force Research Laboratory Wright Site (AFRL/WS) Public Affairs Office (PAO) and is releasable to the National Technical Information Service (NTIS). It will be available to the general public, including foreign nationals.

PAO Case Number: AFRL/WS 06-1135, 01 May 2006.

THIS TECHNICAL REPORT IS APPROVED FOR PUBLICATION.

//Signature//

RYAN J. MORRISSEY
Program Manager
Behavior/Life Prediction Section
Metals Branch
Metals, Ceramics & NDE Division

//Signature//

ROLLIE DUTTON
Chief, Metals Branch
Metals, Ceramics & NDE Division

//Signature//

GERALD J. PETRAK
Assistant Chief, Metals, Ceramics & NDE Division
Materials and Manufacturing Directorate

REPORT DOCUMENTATION PAGE

Form Approved
OMB No. 0704-0188

1. REPORT DATE *(DD-MM-YY)*	2. REPORT TYPE	3. DATES COVERED *(From - To)*
April 2006	Final	02/18/2004 – 03/31/2006

4. TITLE AND SUBTITLE
DEVELOPMENT OF MULTIAXIAL FATIGUE DAMAGE ASSESSMENT METHODS CONSIDERING HIGH CYCLE FATIGUE (HCF)/LOW CYCLE FATIGUE (LCF) INTERACTIONS

5a. CONTRACT NUMBER
FA8650-04-1-5211

5b. GRANT NUMBER

5c. PROGRAM ELEMENT NUMBER
61102F

6. AUTHOR(S)
Dr. Alan R. Kallmeyer (North Dakota State University)
Dr. Peter Kurath (University of Illinois – Urbana-Champaign)

5d. PROJECT NUMBER
2306

5e. TASK NUMBER
A9

5f. WORK UNIT NUMBER
01

7. PERFORMING ORGANIZATION NAME(S) AND ADDRESS(ES)

North Dakota State University
Department of Mechanical Engineering
and Applied Mechanics
1301 12th Avenue N
Fargo, ND 58105-3400

University of Illinois – Urbana-Champaign
Department of Mechanical Engineering
Urbana, IL 61801

8. PERFORMING ORGANIZATION REPORT NUMBER

9. SPONSORING/MONITORING AGENCY NAME(S) AND ADDRESS(ES)
Materials and Manufacturing Directorate
Air Force Research Laboratory
Air Force Materiel Command
Wright-Patterson AFB, OH 45433-7750

10. SPONSORING/MONITORING AGENCY ACRONYM(S)
AFRL-ML-WP

11. SPONSORING/MONITORING AGENCY REPORT NUMBER(S)
AFRL-ML-WP-TR-2006-4112

12. DISTRIBUTION/AVAILABILITY STATEMENT
Approved for public release; distribution is unlimited.

13. SUPPLEMENTARY NOTES
Report contains color.
PAO Case Number: AFRL/WS 06-1135, 01 May 2006.

14. ABSTRACT (*Maximum 200 words*)
The objective of this study was to investigate the interaction between LCF (highly damaging) and HCF (low damage) cycles for a multiaxial stress state. This issue is of great importance in the development of reliable fatigue damage assessment methodologies, as aircraft mission spectra typically contain a large number of HCF cycles coupled with a much smaller number of LCF cycles. Past research in the areas of cycle interactions and damage accumulation have offered contrasting results. Some studies [1-2] have indicated that small cycles (at or near threshold levels) have little effect on the total fatigue life and can be neglected, allowing for use of a linear damage accumulation (Palmgren-Miner) rule. Other studies [3-9], however, have demonstrated that linear damage summation methods may be highly non-conservative, indicating a strong interaction effect exists between LCF and HCF cycles, and the sequence of loading may be an important factor. The majority of these studies were conducted under uniaxial loading conditions, and thus may have limited applicability to multiaxial loadings where non-proportional load paths may alter the interaction. The consideration of cycle interactions within a multiaxial stress state gives rise to some additional challenges, such as cycle definition for non-proportional loadings and the load-path dependence on the interaction effect.

15. SUBJECT TERMS
multiaxial stress, high cycle fatigue (HCF)/low cycle fatigue (LCF)

16. SECURITY CLASSIFICATION OF:			17. LIMITATION OF ABSTRACT:	18. NUMBER OF PAGES	19a. NAME OF RESPONSIBLE PERSON (Monitor)
a. REPORT	b. ABSTRACT	c. THIS PAGE			Ryan J. Morrissey
Unclassified	Unclassified	Unclassified	SAR	32	19b. TELEPHONE NUMBER *(Include Area Code)* N/A

Introduction

The objective of this study was to investigate the interaction between LCF (highly damaging) and HCF (low damage) cycles for a multiaxial stress state. This issue is of great importance in the development of reliable fatigue damage assessment methodologies, as aircraft mission spectra typically contain a large number of HCF cycles coupled with a much smaller number of LCF cycles. Past research in the areas of cycle interactions and damage accumulation have offered contrasting results. Some studies [1-2] have indicated that small cycles (at or near threshold levels) have little effect on the total fatigue life and can be neglected, allowing for use of a linear damage accumulation (Palmgren-Miner) rule. Other studies [3-9], however, have demonstrated that linear damage summation methods may be highly non-conservative, indicating a strong interaction effect exists between LCF and HCF cycles, and the sequence of loading may be an important factor. The majority of these studies were conducted under uniaxial loading conditions, and thus may have limited applicability to multiaxial loadings where non-proportional load paths may alter the interaction. The consideration of cycle interactions within a multiaxial stress state gives rise to some additional challenges, such as cycle definition for non-proportional loadings and the load-path dependence on the interaction effect.

Previous research by the authors [8-9] had demonstrated that a strong HCF/LCF interaction effect existed in Ti-6Al-4V under multiaxial loadings. However, the interaction effect was dependent on load path. In the previous study, two simulated multiaxial mission histories were tested on round bars of Ti-6Al-4V under tension/torsion loading. The histories were constructed by combining a single LCF cycle with several (5 – 50) HCF cycles, as shown in Figure 1. These load paths were selected as they are representative of actual service events observed in aircraft engine materials. Load levels were chosen to produce LCF lives in the range of 10^4 – 10^5 cycles and HCF lives in the range of 10^8 – 10^9 cycles. The ratios of HCF to LCF lives (N_{HCF}/N_{LCF}) used in this study are representative of service conditions, although actual load levels may differ. The results of this test program produced some interesting findings. Independently, the LCF cycles in the two histories had roughly equivalent fatigue lives (based on experimental results), and predicted fatigue lives for the HCF cycles were similarly equivalent. However, when combined, the "Box-1" mission demonstrated a strong, nonlinear interaction effect between the LCF and HCF cycles, whereas the "Check-1" mission exhibited no discernable interaction effect.

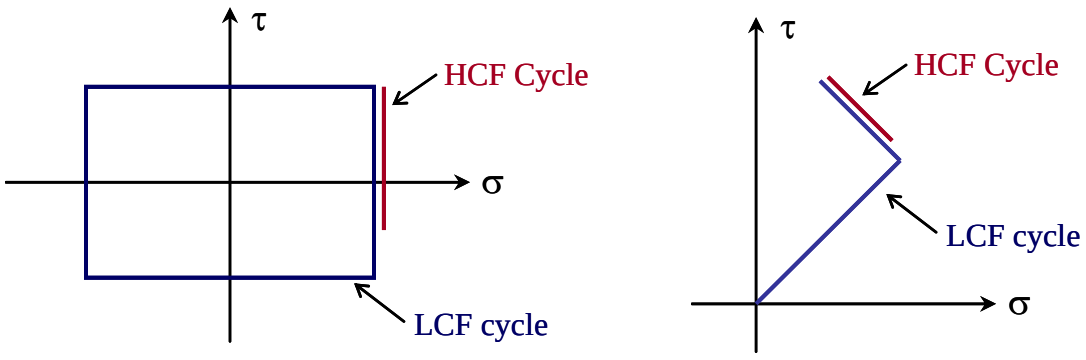

Figure 1. Mission histories used in a previous study, showing LCF and HCF cycles for the "Box-1" path (left) and the "Check-1" path (right).

It was initially theorized that the observed difference in the interaction effect was due to the specific stress values occurring on the "critical plane" for each load path. That is, mission histories in which the LCF and HCF critical planes (planes on which fatigue damage is maximized according to some predefined criterion) coincide would be expected to show a greater interaction effect than histories in which the critical planes did not coincide. The authors were somewhat successful in modeling the observed behavior in this limited study [8-9] by utilizing the Findley "critical-plane" multiaxial fatigue parameter [10] in conjunction with a nonlinear cumulative damage model put forth by Manson and Halford [4-5]. The Findley Parameter (FP), shown in Eq. (1), assumes that the cyclic shear stress on a plane is the primary cause of fatigue crack initiation, but that the maximum normal stress on the plane plays a secondary influence by opening the crack (if tensile), thereby reducing friction and increasing the damage caused by the shear stress.

$$FP = \tau_a + k\sigma_{\max} = f(N_f) \tag{1}$$

It was also noted that such a distinction in the interaction effect between load paths could not be accounted for using a traditional equivalent (invariant) stress type of parameter.

By calculating the Findley parameter on each plane, it was found that the LCF and HCF critical planes (defined by the maximum value of the Findley parameter) were in very close proximity for the Box-1 path, but not for the Check-1 path. Furthermore, by using the Damage Curve Approach (DCA) developed by Manson and Halford [4-5], the fatigue lives of the Box-1 mission could be predicted. The DCA is a nonlinear cumulative damage model capable of accounting for load sequence and interaction effects. Using this model, the fatigue damage corresponding to n cycles applied at a loading with a fatigue life of N_f is calculated as

$$D = \left(\frac{n}{N_f} \right)^{\left(\frac{N_f}{N_{ref}} \right)^{\alpha}} \tag{2}$$

where α is a material parameter that accounts for the degree of nonlinearity, and N_{ref} represents the life at which damage accumulates linearly. For simplicity, Manson and Halford [4-5] generally assumed $N_{ref} = 1$, arguing that, for calculation purposes, damage could be assumed to accumulate linearly within a single cycle of loading.

Based on the results of the initial study, additional mission histories were constructed that would either verify or refute the critical plane hypothesis. These histories were constructed with the primary consideration of varying the location of the HCF critical plane relative to the LCF critical plane, using the Findley parameter (and other similar models) to define the fatigue damage. The testing and analysis of these new mission histories forms the basis of the present study. The details of the experimental testing, results, analysis and conclusions are explained in the following sections.

Experimental Results

Fourteen biaxial specimens of Ti-6Al-4V were supplied by AFRL to the University of Illinois for the experimental phase of this study. The specimens had a solid cross-section of 12.5 mm diameter, and were machined and finished following the same procedures used in the earlier HCF program. All specimens were tested on a biaxial (tension/torsion) load frame in strain control. Since the specimens were solid rather than hollow, the stress and strain values referenced in this report represent maximum (surface) values. In certain tests, the specimens experienced small-scale yielding on the surface during the first reversal. In these cases, surface stresses were determined from the measured strain values using an elastic-plastic finite element analysis performed in Ansys. This analysis utilized a multilinear kinematic hardening rule in conjunction with the cyclic stress-strain equation (Ramberg-Osgood) for Ti-6Al-4V:

$$\varepsilon = \frac{\sigma}{E} + \left(\frac{\sigma}{K'}\right)^{1/n'} \tag{3}$$

In the FEA analysis, the following cyclic material properties were used: E = 16.98 Msi, G = 6.29 Msi, ν = 0.349, K' = 124 ksi, n' = 0.0149, and the cyclic yield strength σ_y' = 109.22 ksi.

Of the fourteen specimens received from AFRL, one was tested as a repeat baseline multiaxial test to verify the similarity of materials between these specimens and those tested in the HCF program. One other specimen experienced control problems during the test, and is therefore considered an invalid test. Thus, twelve additional valid mission history tests were conducted, as described below.

The new mission histories constructed for this study are shown in Figure 2. In all cases, the LCF cycles corresponded to load paths tested in the previous study, so the experimental LCF lives were known. The LCF lives for these load paths are all in the same order of magnitude, ranging from approximately 43,000 to 74,000 cycles. The HCF cycles, in shape and stress level, were generally defined to result in fatigue lives of $10^8 - 10^9$ cycles (based on model predictions), but to generate differing conditions of critical plane orientation between the LCF and HCF cycles. Based on the results of the initial study, the Findley parameter was used to make fatigue life predictions for the HCF cycles and to identify the critical plane orientation for both the LCF and HCF cycles. The baseline sets of uniaxial and biaxial Ti-6Al-4V data used for calibration of the Findley model are shown in Figure 3.

The experimental results from the current test program are shown in Table 1, along with the mission-history results from the initial HCF program. Most mission histories consisted of 1 LCF and 50 HCF cycles, although the Box-1B path contained 1 LCF and 5 HCF cycles. The difference between the Tor-Ax 1 and 2 paths was only in the size of the subcycle. The HCF lives shown in Table 1 were calculated using the Findley parameter. Note that the majority of these lives represent extrapolations beyond the current data set shown in Fig. 3. In addition, since the curve is very flat in this region, small changes in stress levels cause large variations in predicted lives. Thus, although the predicted HCF lives in Table 1 vary, they all had similar values of the Findley parameter (with the exception of the Tor-Ax 2 and Tor-Pro histories).

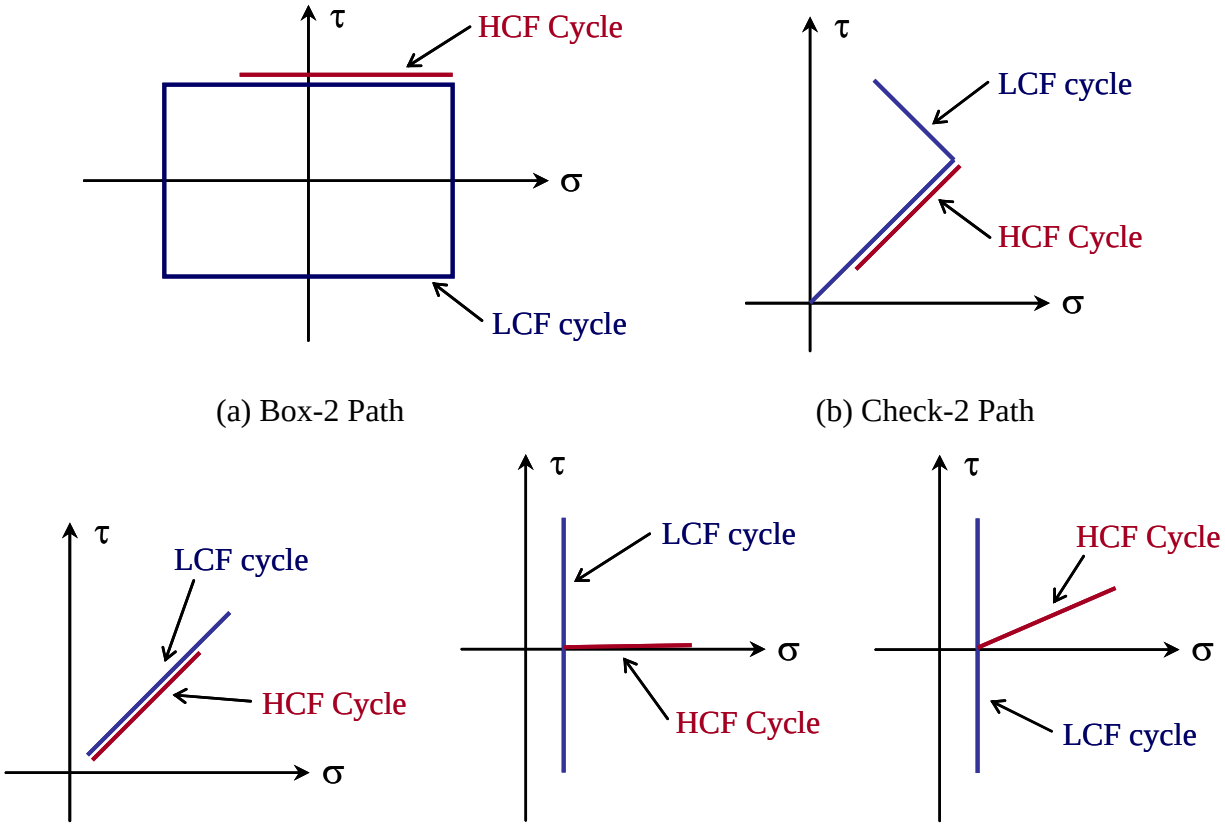

(a) Box-2 Path (b) Check-2 Path

(c) Proportional Path (d) Tor-Ax Path (e) Tor-Pro Path

Figure 2. Mission histories tested in the current study, showing LCF and HCF cycles.

As is evident from Table 1, there is a significant HCF/LCF interaction effect present in these multiaxial mission histories; however, the degree of interaction is heavily path dependent. For all histories except Tor-Pro, a simple cumulative damage analysis based on the Palmgren-Miner rule with $N_{LCF} \approx 50{,}000$ and $N_{HCF} \approx 10^8$ predicts very little effect from the HCF cycles; i.e., these mission histories would be expected to be dominated by the LCF cycles. A linear damage analysis of the Tor-Pro history results in a predicted mission life of 27,000 cycles (roughly 3× reduction in LCF life). However, in some of these cases, the presence of the HCF cycles caused mission lives to be reduced by over an order of magnitude relative to the LCF lives. In other histories, there was little or no discernable effect. The actual half-life stress and strain values from the mission history tests are included in Appendix A.

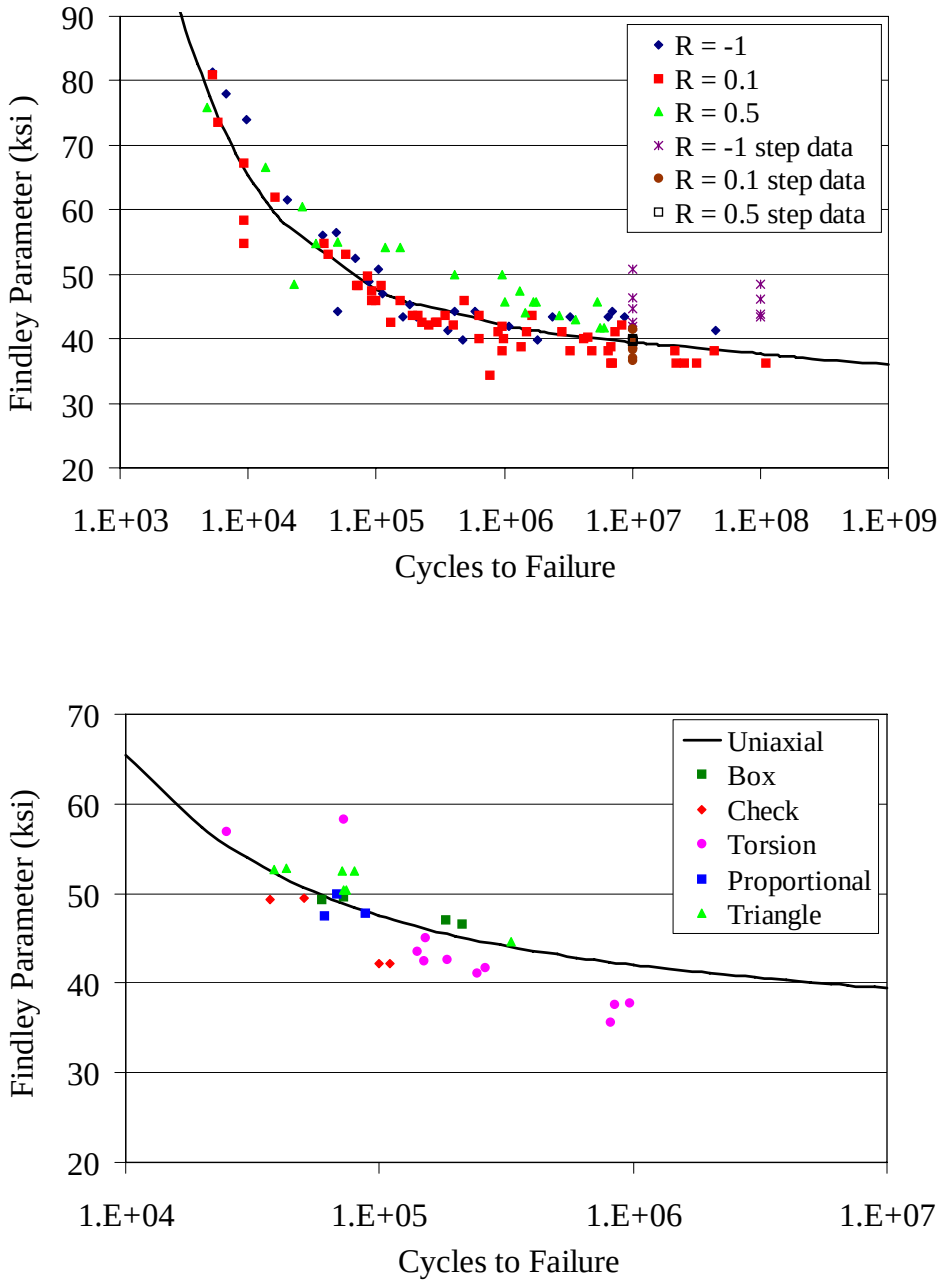

Figure 3. Correlation of Ti-6Al-4V uniaxial data (top) and biaxial data (bottom) using the Findley parameter, from the initial HCF program.

Table 1
Mission History (LCF/HCF) Experimental Results

History	Specimen ID's	LCF/HCF cycles	Average LCF Life	Predicted HCF Life	Avg. Mission Life	$N_{LCF}/N_{Mission}$
Box-1A	142-7* 178-6*	1 / 50	68,721	2.2×10^8	20,446	3.4
Box-1B	142-1* 178-9*	1 / 5	68,721	2.2×10^8	44,133	1.6
Box-2	03-609 03-611 03-610	1 / 50	68,721	6.3×10^8	10,927	6.3
Check-1	178-4* 142-3*	1 / 50	43,744	2.9×10^8	47,160	0.9
Check-2	03-613 03-612	1 / 50	43,744	2.6×10^8	7,250	6.0
Proportional	04-B00 04-A97	1 / 50	74,217	2.6×10^8	54,728	1.4
Tor-Ax 1	04-195 04-A99	1 / 50	72,926	9.8×10^7	3,688	19.8
Tor-Ax 2	04-A96	1 / 50	72,926	$> 1 \times 10^{10}$	6,470	11.3
Tor-Pro	04-A93 04-A95	1 /50	72,926	2.2×10^6	2,944	24.8

* Samples tested in initial HCF program.

Preliminary Critical Plane Analysis

It was initially postulated that the differences in the observed HCF/LCF interactions can be explained using the critical plane concept. That is, interaction effects will be greater when the HCF and LCF critical damage planes coincide. To evaluate this hypothesis, an initial analysis was performed using the Findley parameter (Eq. 1) as the basis for calculating fatigue damage on each plane for both the LCF and HCF cycles. As previously mentioned, this assumes that crack initiation is driven primarily by cyclic shear stresses; thus, critical planes will typically be those which experience a large alternating shear stress. The Findley parameter was used initially due to its reasonable correlation with multiaxial test data for Ti-6Al-4V [8, 9]. The value of k used here was 0.379, which was obtained through a least-squares error minimization technique applied to the uniaxial Ti-6Al-4V data; i.e., k was calculated by collapsing the uniaxial data at different stress (R) ratios.

The variation of the Findley parameter with plane orientation for both the LCF and HCF cycles is shown for the Box-1 and Check-1 paths (tested in the initial HCF study) in Figures 4 and 5. Note that for both missions, the peak value of the Findley parameter (FP) is approximately 49 ksi for the LCF cycle and 37 ksi for the HCF cycle. For the Box-1 path (Fig. 4), there are four LCF critical plane regions where the FP reaches a peak, indicated by the dashed lines. In this path, a peak in the HCF curve corresponds to one of the LCF critical planes, indicating higher HCF damage on an LCF critical plane. The Check-1 path (Fig. 5) contains

only two LCF peaks in the FP. In this path, the HCF peak does not correspond directly to an LCF peak. Thus, it would be expected that the HCF/LCF interaction effect would be smaller in the Check-1 path than the Box-1 path, which agrees with the experimental results.

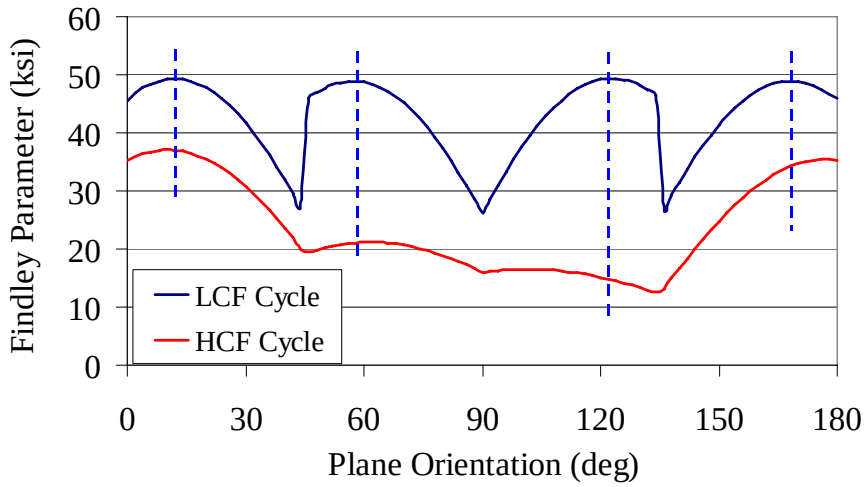

Figure 4. Variation of Findley parameter with plane orientation for the Box-1 path.

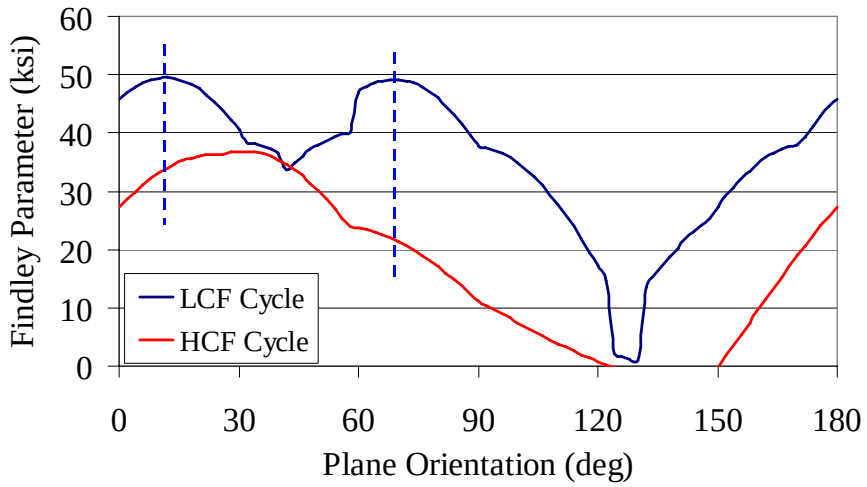

Figure 5. Variation of Findley parameter with plane orientation for the Check-1 path.

Based on the findings for the Box-1 and Check-1 paths, the Box-2 and Check-2 paths were defined to further explore the relationships between LCF and HCF critical planes. The variation of the LCF and HCF Findley parameters with plane orientation for these two paths is shown in Figures 6 and 7. As with the previous paths, the peak value of the Findley parameter (FP) for the Box-2 and Check-2 paths is approximately 49 ksi for the LCF cycle and 37 ksi for the HCF cycle. For the Box-2 path (Fig. 6), the HCF peak occurs between two LCF peaks. In the Check-2 path (Fig. 7), the LCF and HCF peaks nearly coincide. Thus, it was expected that the Box-2 path would show negligible HCF/LCF interactions and the Check-2 path would show

a high degree of interaction. While the experimental results for the Check-2 path matched expectations, the results for the Box-2 path demonstrated the opposite trend, as shown in Table 1.

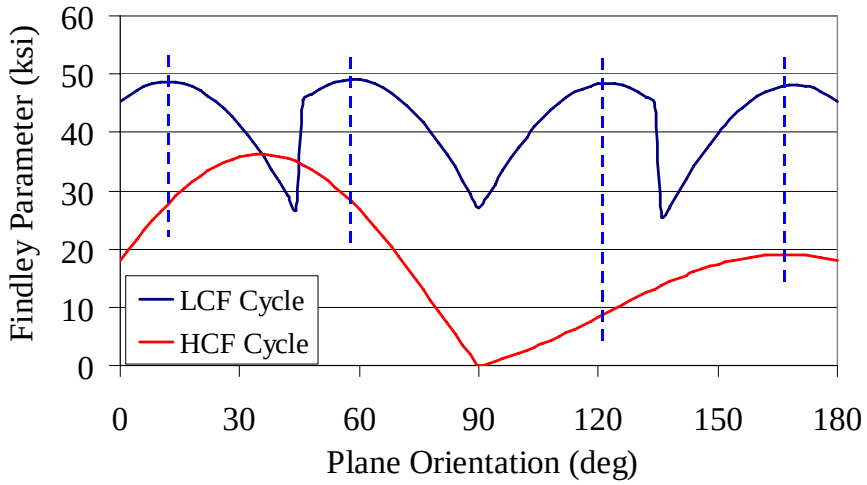

Figure 6. Variation of Findley parameter with plane orientation for the Box-2 path.

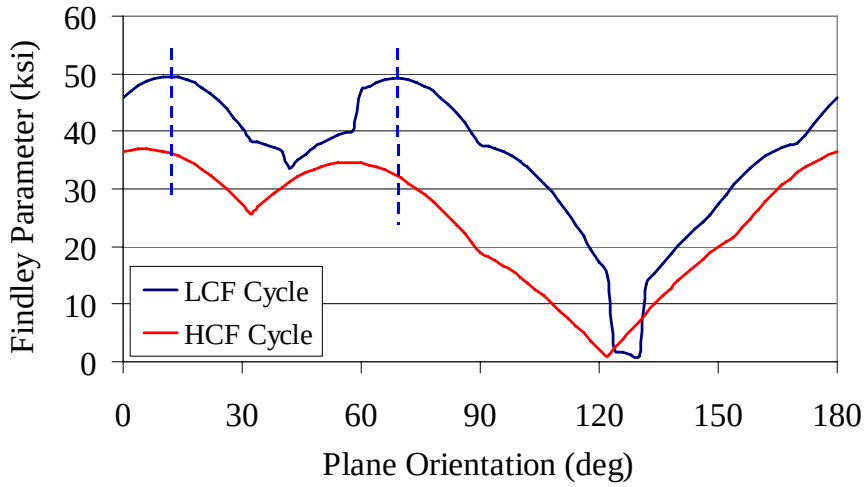

Figure 7. Variation of Findley parameter with plane orientation for the Check-2 path.

The findings from the preliminary analysis do not fully confirm the original hypothesis that interactions will be maximized when LCF and HCF critical planes coincide, based on a common definition of a damage parameter. This was further verified through testing of the Proportional mission history, which was constructed to specifically control the relative orientations of the LCF and HCF critical planes. For this mission, the LCF and HCF cycles are identical in shape; thus, their critical planes will exactly coincide. According to the original hypothesis, the Proportional mission would therefore be expected to see significant HCF/LCF interactions. However, the experimental results demonstrated just the opposite, with little observed life reduction in this mission history. Consequently, the original hypothesis was deemed inadequate to explain the observed results.

Refined Critical Plane Analysis

The experimental findings suggest that different damage mechanisms may be responsible for the varying levels of HCF/LCF interactions in the multiaxial load paths. Based on the results of the preliminary analysis, another multiaxial mission history (Tor-Ax) was designed to emphasize differing damage mechanisms between the LCF and HCF cycles. In this load path, the LCF cycle is fully reversed torsion (with a small mean tensile stress) while the HCF cycle is cyclic tension (with no shear). Thus, the 0° plane experiences the largest alternating shear stress from the LCF cycles and also the largest alternating tensile stress from the HCF cycles. The experimental results indicate a high degree of LCF/HCF interactions occurred in this history; i.e., there was a significant reduction in mission life due to the presence of the HCF cycles. These results suggest that a coupling of shear-dominated damage from the LCF cycles and tensile-dominated damage from the HCF cycles may result in maximum interactions.

Physically, this observation can be explained by the hypothesis that the LCF cycles first initiate microcracks through shear-driven mechanisms (mode II growth), and the HCF cycles then contribute to an increased rate of crack propagation due to cyclic tensile stresses (mode I growth) on planes at or near the LCF critical plane orientations. For load paths in which the HCF maximum tensile planes coincide with the LCF maximum shear planes, the LCF-initiated shear cracks would not need to change direction to be propagated in tension by the HCF cycles. Thus, there would be lesser resistance to the evolution of the mode II (shear) cracks into mode I (tensile) cracks.

This hypothesis is also consistent with a number of other experimental studies of load-sequence effects [3-5] under uniaxial loading, in which it has been found that high-low load sequences (LCF-HCF sequences) emphasize non-linear (accelerated) damage accumulation much more than low-high load sequences (HCF-LCF sequences). Thus, LCF cycles must first initiate the cracks before the HCF cycles can contribute to the damage by accelerated crack growth. In the case of repeating histories, as in this test program, the LCF-HCF sequence may dominate the HCF-LCF sequence.

It should also be noted that, given the ratio of the number of LCF cycles to HCF cycles within a mission (1/50), the histories tested in this study are all dominated by LCF damage. Thus, a reduction in LCF life due to HCF accelerated crack growth, rather than an increase in HCF life associated with periodic LCF overload effects (due to crack tip blunting, residual stresses, and crack closure) is plausible. This would also be in agreement with other studies that have shown that cyclic stresses below the endurance limit or threshold stress intensity cause a reduction in life in variable load histories [7].

To further examine the new hypothesis, another critical plane analysis was performed to identify the LCF and HCF damage as a function of plane orientation for each of the mission histories, but using alternate definitions for the LCF and HCF damage parameters. A new damage parameter, developed by the authors [11], has been shown to provide an improved correlation of the uniaxial and multiaxial test data for Ti-6Al-4V. Similar to the Findley parameter, the new damage parameter assumes that cracks nucleate through shear-driven mechanisms, with normal stresses contributing in a secondary role by influencing crack-face interaction during shear growth. A second term accounts for additional damage caused by cyclic normal stresses on the critical plane within the dominant shear cycle. This new parameter is expressed as

$$DP = \tau_{\max}\left(1-\frac{\tau_{\min}}{\tau_{\max}}\right)^{w_1}\left(1+\frac{k_1\sigma_{\tau\max}+k_1\sigma_{\tau\min}}{\sigma_y}\right)+k_2\sum\sigma^{+}_{\max}\left(1-\frac{\sigma^{+}_{\min}}{\sigma^{+}_{\max}}\right)^{w_2} \quad (4)$$

$$\text{where } k_1 = \begin{cases} k_1^{+} \; if \; \sigma > 0 \\ k_1^{-} \; if \; \sigma < 0 \end{cases}$$

In Eq. (4), τ_{max} and τ_{min} are the shear reversal points on the critical plane, and $\sigma_{\tau max}$ and $\sigma_{\tau min}$ are the corresponding normal stresses on this plane at the instant of shear reversal. These stresses are divided by the yield strength, σ_y, to maintain consistency of units. In the second term, σ_{max} and σ_{min} are the maximum and minimum normal stresses on the critical plane over the entire cycle. The σ^+ notation indicates that only positive (tensile) values are used in the equation. If σ_{min} or σ_{max} is negative, that value is set to zero in Eq. (4).

The first term in Eq. (4) accounts for a mean shear stress effect, with the multiplier acting to modify this value to account for crack face interaction due to the normal stresses at the shear reversals. The definition of the k_1 term allows for a different influence of tensile and compressive stresses. The last term accounts for the additional damage caused by cyclic tensile stresses on the critical plane. If multiple normal stress cycles exist within the shear cycle, their contribution is included through the summation in this term. The values of k_1, w_1, k_2 and w_2 are fit by collapsing uniaxial and multiaxial fatigue data. In this analysis, w_2 was taken to be 0.5 and k_1, w_1, and k_2 were determined by fitting the combined data for Ti-6Al-4V on the plane of maximum alternating shear stress, resulting in the following values:

$$k_1^{+} = 0.749, \quad k_1^{-} = 0.065, \quad w_1 = 0.679, \quad k_2 = 0.158, \quad w_2 = 0.5 \quad (5)$$

The resulting fits of the uniaxial and biaxial Ti-6Al-4V fatigue data are shown in Figures 8 and 9. The plane of maximum alternating shear stress (max shear plane) was defined as the critical plane in this analysis in order to simplify the optimization of the parameters shown in Eq. (5). When the critical plane is defined as the plane of maximum damage (i.e., the plane with the highest value of DP from Eq. (4)), the orientation of the plane itself may change as the values of the k and w terms are varied. From a practical standpoint, the max shear plane is also easier to locate under general loading conditions than the max damage plane, simplifying the implementation of the damage parameter in a general design algorithm. Comparing Figures 8 and 9 to Figure 3, it is evident that the use of the damage parameter shown in Eq. (4) on the max shear plane results in a very good overall correlation of both the uniaxial and multiaxial fatigue data. It should also be noted that, in most cases, the max damage plane is very near the max shear plane (generally within 10°). Consequently, this new damage parameter was used to model the LCF cycles in the updated critical plane analysis of the mission histories, as described below.

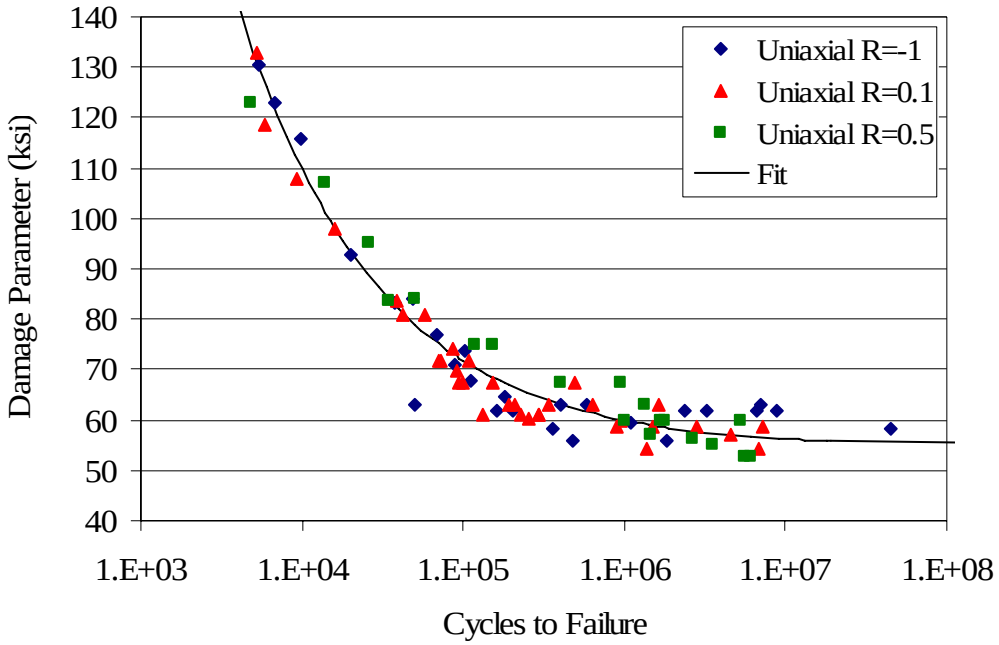

Figure 8. Correlation of Ti-6Al-4V uniaxial data using Eq. (4).

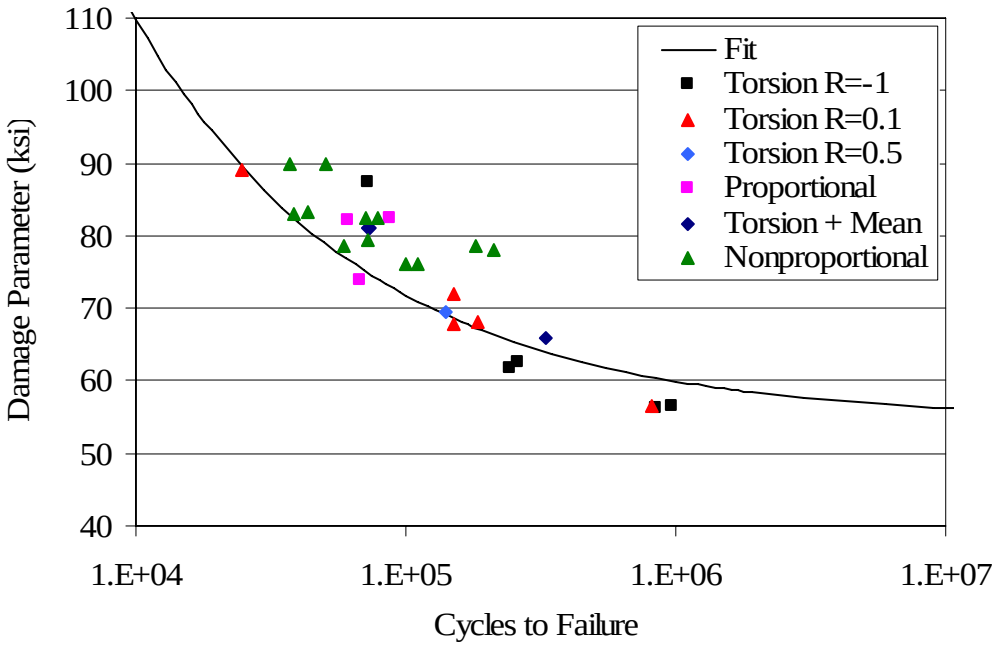

Figure 9. Correlation of Ti-6Al-4V biaxial data using Eq. (4).

Based on the hypothesis that the HCF cycles contribute to an increased rate of mode I crack propagation, the HCF damage in the refined analysis was computed in terms of a "Walker" stress parameter [12], defined as

$$DP = \sigma^{+}_{\max}\left(1 - \frac{\sigma^{+}_{\min}}{\sigma^{+}_{\max}}\right)^{w} \tag{6}$$

where the σ^{+} notation indicates that only tensile values of normal stress are used, and w was taken as 0.5. The critical plane for this parameter was defined as the plane of maximum alternating tensile (principal) stress, consistent with mode I crack growth. This parameter was adopted to represent the HCF damage since the Walker relationship (in terms of stress intensity factors) is often used in crack growth studies to account for mean stress effects. Thus, it would be expected that the crack growth rate would roughly scale with the value of this parameter. Here, the variation in the HCF DP with plane orientation is simply used to compare, on a relative basis, the potential for crack growth due to the HCF cycles on a particular plane. Note that there is no direct correlation between the magnitudes of the LCF and HCF damage parameters used in this analysis.

Plots of the LCF DP (from Eq. (4)) and the HCF DP (from Eq. (6)) vs. plane orientation for the Box-1, Check-1, Box-2, Check-2, and Proportional missions are shown in Figures 10 – 14. In these figures, the LCF critical planes based on the max shear stress range ($\Delta\tau$) are indicated by dashed purple lines, and the LCF critical planes based on the maximum damage are indicated by dashed green lines. Note that the maximum damage planes are typically within 10° of the maximum shear planes. The maximum value of the HCF DP in each mission history is also indicated on the figures.

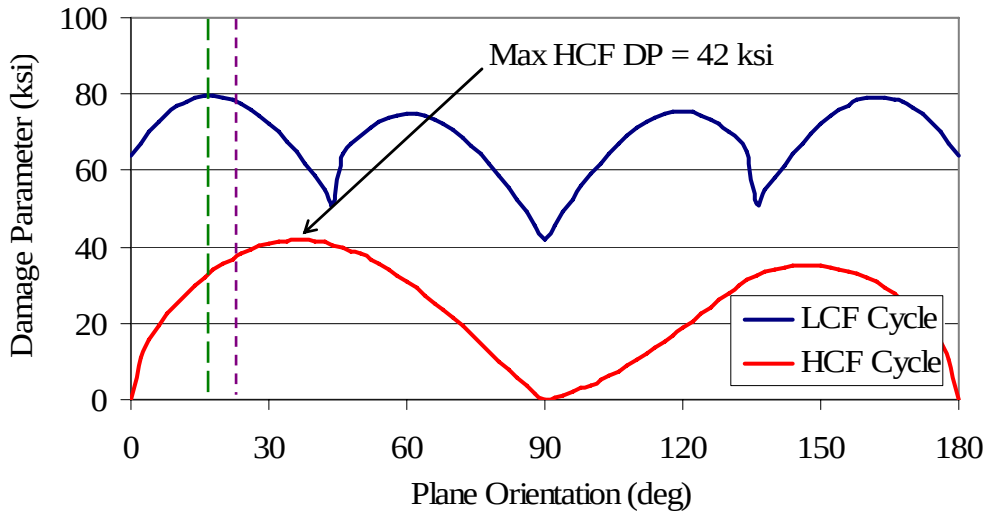

Figure 10. Variation of the LCF and HCF damage parameters with plane orientation for the Box-1 path. The purple line indicates the critical LCF max shear plane, and the green line indicates the critical LCF max damage plane.

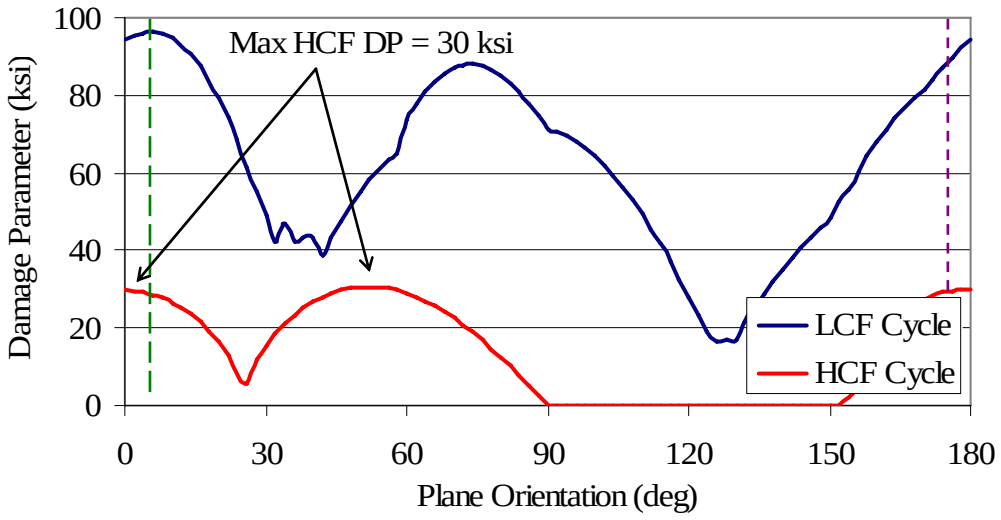

Figure 11. Variation of the LCF and HCF damage parameters with plane orientation for the Check-1 path. The purple line indicates the critical LCF max shear plane, and the green line indicates the critical LCF max damage plane.

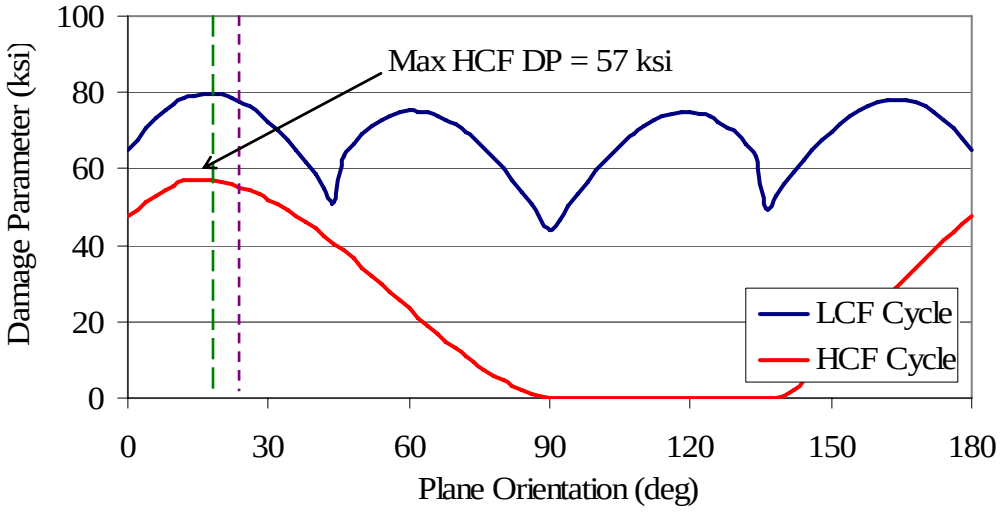

Figure 12. Variation of the LCF and HCF damage parameters with plane orientation for the Box-2 path. The purple line indicates the critical LCF max shear plane, and the green line indicates the critical LCF max damage plane.

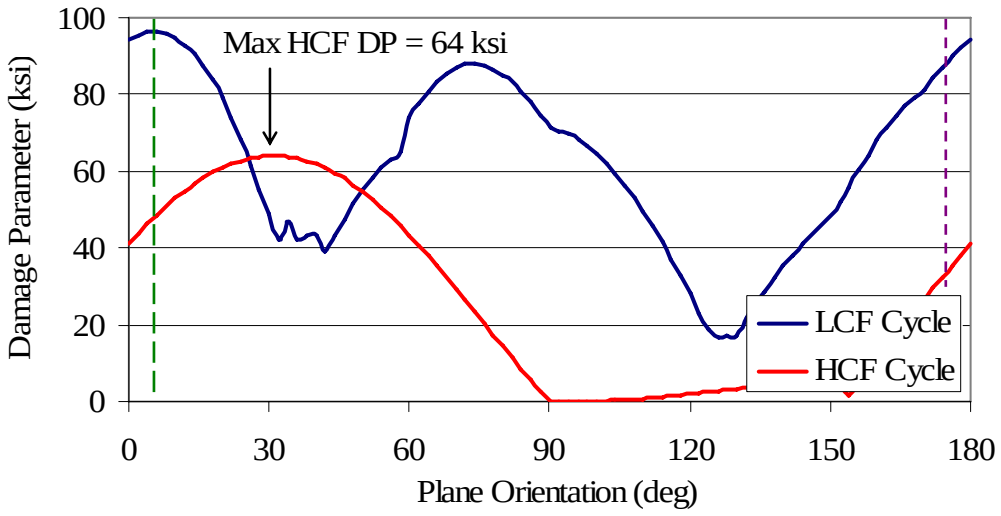

Figure 13. Variation of the LCF and HCF damage parameters with plane orientation for the Check-2 path. The purple line indicates the critical LCF max shear plane, and the green line indicates the critical LCF max damage plane.

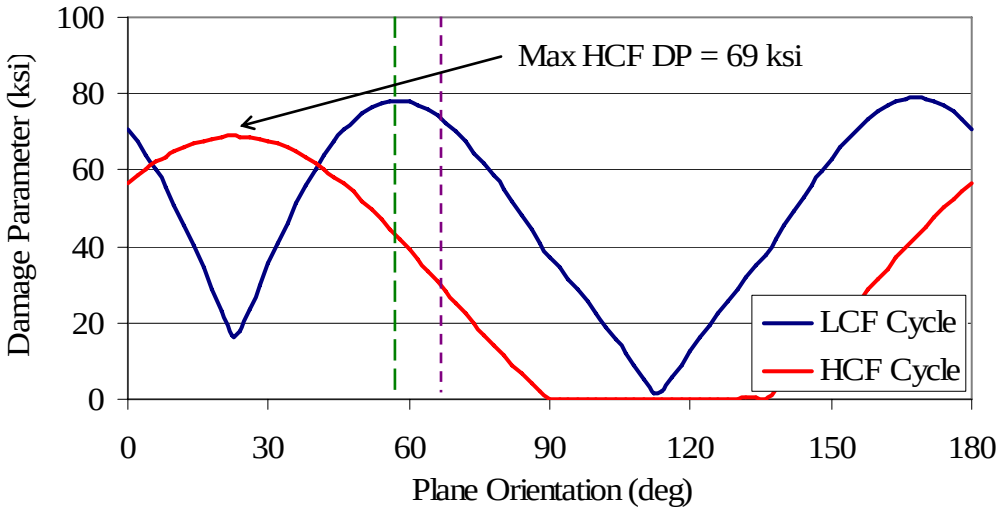

Figure 14. Variation of the LCF and HCF damage parameters with plane orientation for the Proportional path. The purple line indicates the critical LCF max shear plane, and the green line indicates the critical LCF max damage plane.

A comparison of the results shown in Figures 10 – 13 with those from Figures 4 – 7 appears to support, qualitatively, the hypothesis that the LCF/HCF interaction effect is caused by HCF crack growth of LCF initiated damage. Note, however, that this interaction mechanism does not necessarily require the LCF and HCF critical planes to coincide. As previously

discussed, it would be anticipated that the interaction effect would be maximized if the planes do coincide since no crack turning would be required. However, it is also recognized that cracks may initiate on one plane and then turn and propagate on another, as is typically the case under uniaxial loading conditions. Thus, the level of interaction (magnitude of LCF life reduction due to the HCF cycles) would be primarily dependent on the peak value of the HCF damage parameter, with a lesser dependence on the orientation of the HCF critical plane relative to the LCF critical plane.

Examination of the HCF DP values shown in Figures 10 – 14 indicates a reasonably good correlation with the magnitude of the mission (LCF) life reduction. For example, in the Check-1 path (Fig. 11), the maximum value of the HCF damage parameter is 30 ksi. No reduction in LCF life was observed experimentally in this mission history, indicating the HCF cycle was too small to propagate any LCF initiated damage. In the Box-1 path (Fig. 10), the maximum HCF DP is 42 ksi, corresponding to a factor of 3 reduction in LCF life (Box-1A). For the Box-2 and Check-2 paths (Figs. 12 and 13), the maximum HCF DP values were 57 – 64 ksi, corresponding to a life reduction of a factor of 6. Thus, these results all follow a general trend of increasing life reduction with increasing HCF DP. The only anomaly to the trend was in the Proportional path (Fig. 15). In this case, the maximum HCF DP value was 69 ksi, but the life reduction was only a factor of 1.4.

The good correlation of the experimental results for the Box, Check, and Proportional missions with the new damage hypothesis lead to the development of the Tor-Ax path, as previously discussed. The resulting variation of the LCF and HCF damage parameters with plane orientation for the Tor-Ax 1 and 2 missions are shown in Figures 15 and 16, respectively. The results for these missions are consistent with the previous missions. The maximum HCF DP in the Tor-Ax 2 path is 58 ksi, corresponding to a factor of 11 reduction in life. This reduction is within a factor of 2 of that found for the Box-2 and Check-2 paths. For the Tor-Ax 1 path, the maximum HCF DP was 72 ksi, corresponding to a life reduction of a factor of 20.

To further study the influence of critical plane orientation between the LCF and HCF cycles, the Tor-Pro mission history was constructed. In this mission, the LCF cycle was identical to that in the Tor-Ax missions. The HCF cycle was defined to produce the same value on the LCF critical plane as in the Tor-Ax 2 path, but the same maximum value as in the Tor-Ax 1 path (although on a different plane), as shown in Figure 17. Thus, if the life reduction for this mission was the same as the Tor-Ax 2 path, this would indicate that the relative orientation of the LCF and HCF critical planes was very important. Conversely, if the life reduction for the mission was the same as the Tor-Ax 1 path, this would indicate that a mode II crack could easily turn into a mode I crack with little resistance, regardless of plane orientation.

As shown in Table 1, the experimental life reduction for the Tor-Pro mission was approximately a factor of 25, similar to that for the Tor-Ax 1 mission. Based on this result, it is concluded that it is the overall magnitude of the HCF DP that primarily dictates the level of LCF/HCF interaction in this material. The orientation of the LCF and HCF critical planes appears to play a lesser role in defining the magnitude of the interaction effect.

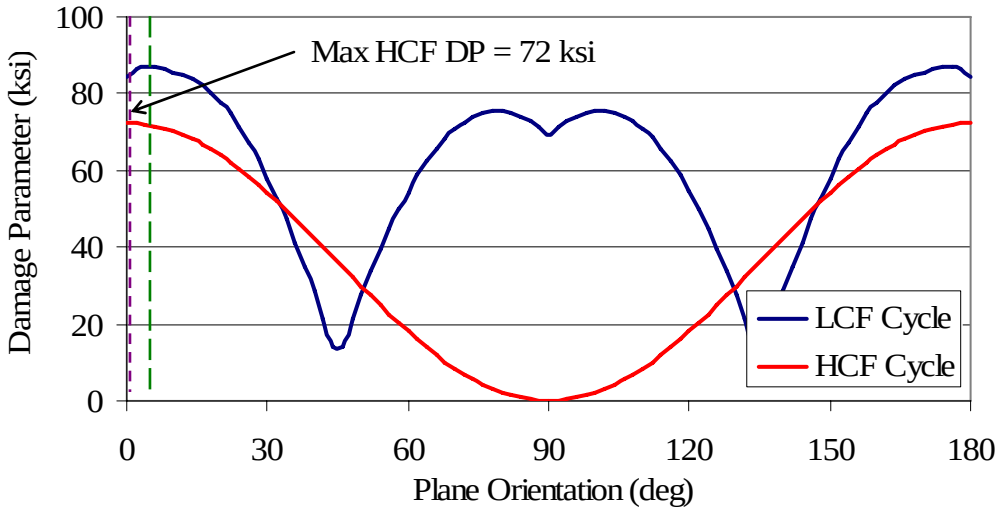

Figure 15. Variation of the LCF and HCF damage parameters with plane orientation for the Tor-Ax 1 path. The purple line indicates the critical LCF max shear plane, and the green line indicates the critical LCF max damage plane.

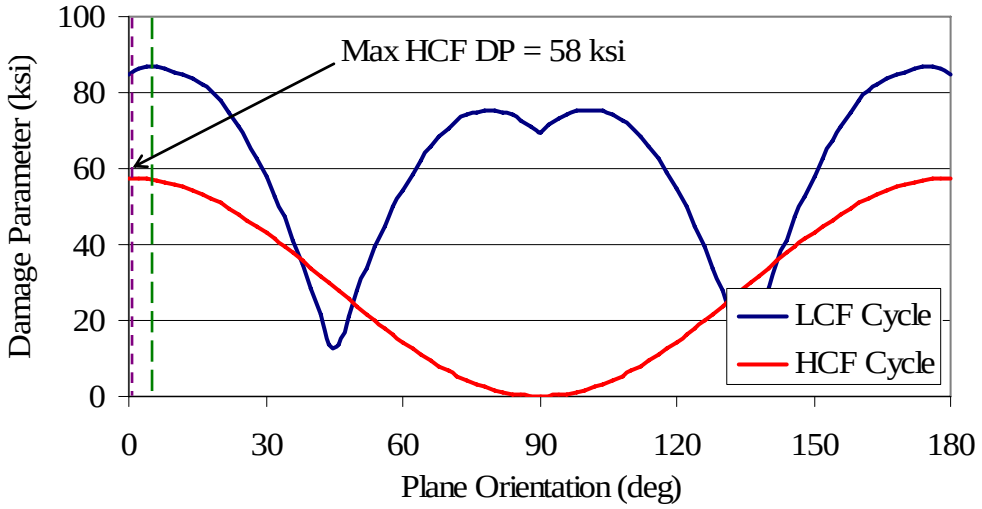

Figure 16. Variation of the LCF and HCF damage parameters with plane orientation for the Tor-Ax 2 path. The purple line indicates the critical LCF max shear plane, and the green line indicates the critical LCF max damage plane.

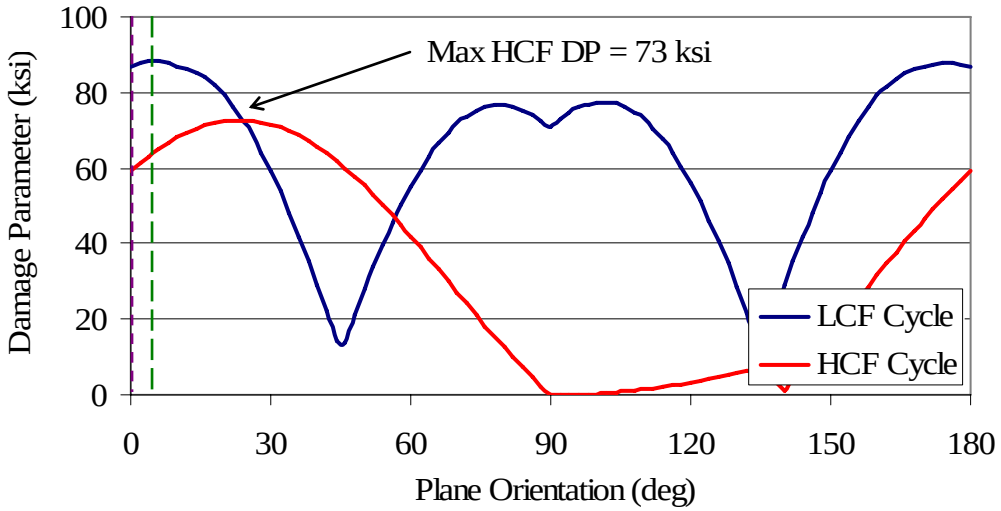

Figure 17. Variation of the LCF and HCF damage parameters with plane orientation for the Tor-Pro path. The purple line indicates the critical LCF max shear plane, and the green line indicates the critical LCF max damage plane.

Overall, the results presented in this study demonstrate a trend of increasing HCF/LCF interaction (reduced mission life) with increasing magnitude of HCF tensile damage, regardless of plane orientation. A possible explanation for the smaller interaction effect observed in the Proportional path, despite the relatively high magnitude of HCF damage, may be due to the presence of an "overload" effect from the LCF cycles during HCF crack propagation. It is well known that high tensile loads (overloads) often cause a subsequent retardation in the crack growth rate at lower load levels due to crack tip plasticity (resulting in compressive residual stresses), crack closure, crack tip blunting, etc. In the Proportional path, the peak tensile stress from the LCF cycle on the HCF critical plane was 94 ksi, which was considerably larger than the peak LCF tensile stress on an HCF critical plane in any of the other mission histories. Note from Figure 2(c) that the HCF cycle was defined as the lower portion of the LCF cycle. Thus, the LCF cycle may have acted as a periodic tensile overload during HCF crack propagation, causing a retardation in the crack growth which mitigated the life reduction.

The explanation for the observed LCF/HCF interaction effect presented here is consistent with the findings of other researchers on the subject of load sequence effects, notably that a greater life reduction is observed when large cycles are applied first, followed by small cycles. This implies that damage (microcracks) must first be initiated by the large (LCF) cycles before the smaller (HCF) cycles will have an adverse effect by contributing to the growth of that damage. For the mission histories tested in this program, which consisted of repeated blocks of 1 LCF cycle and 5 – 50 HCF cycles, it is likely that early in the life the HCF cycles contributed very little to the damage accumulation. However, once enough LCF cycles (missions) had been applied to nucleate a small crack, it is probable that the HCF cycles became much more important in the propagation of the crack. At that point, the LCF cycles would have a much smaller influence, except in the cases where they created tensile overloads on the HCF growth planes as noted above.

Experimental Crack Plane Measurements

In an effort to further assess the validity of the damage parameters used in this analysis, as well as the argument that the HCF cycles propagate LCF-induced damage, rough measurements were made of the plane orientations at which cracks initiated and propagated in the specimens tested in this study. In the majority of the ½ in diameter specimens, the crack growth planes were easily identifiable, and in some cases the crack initiation planes were also discernable. However, in some specimens, crack initiation planes were difficult to determine due to obliteration during subsequent loading.

Micrographs were taken of each specimen using a digital microscope with 50× magnification. Representative micrographs, taken from the side view to identify the crack plane orientations, are shown in Figures 18 – 23. The specimens tested in the original HCF study (Box-1 and Check-1 paths) were not available; thus, no crack plane measurements were obtained for these mission histories. The observed crack initiation and propagation plane orientations, measured from these micrographs, are summarized in Table 2, along with the predicted crack plane orientations for crack initiation (LCF cycle) and propagation (HCF cycle) taken from Figures 10 – 17. The predicted crack initiation planes shown in Table 2 are based on the maximum value of the LCF DP from Eq. (4) rather than the maximum shear plane. In all cases, several measurements were taken from different views, and the results averaged to give the values shown in Table 2.

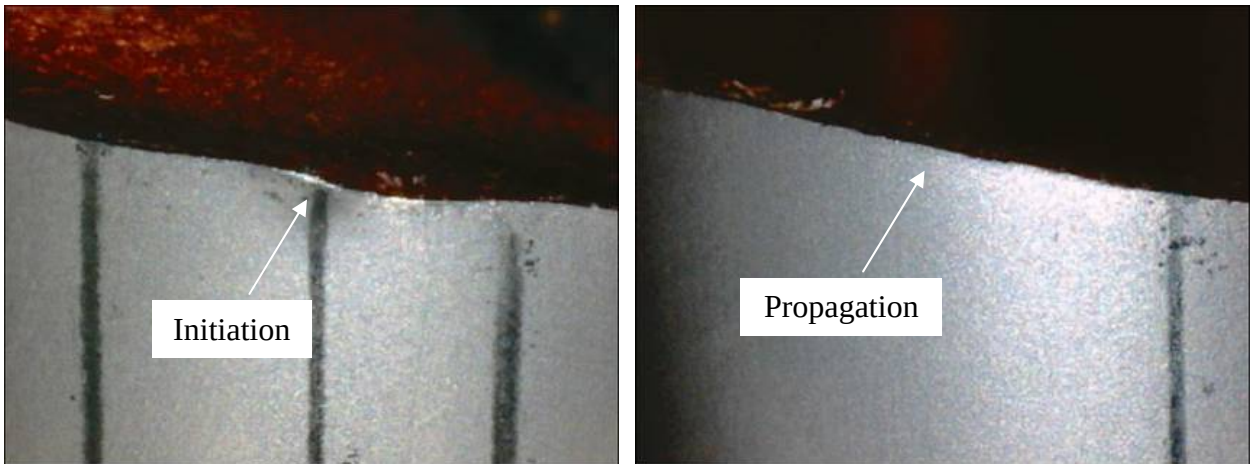

Figure 18. Crack initiation and propagation planes in Specimen 03-609: Box-2 path.

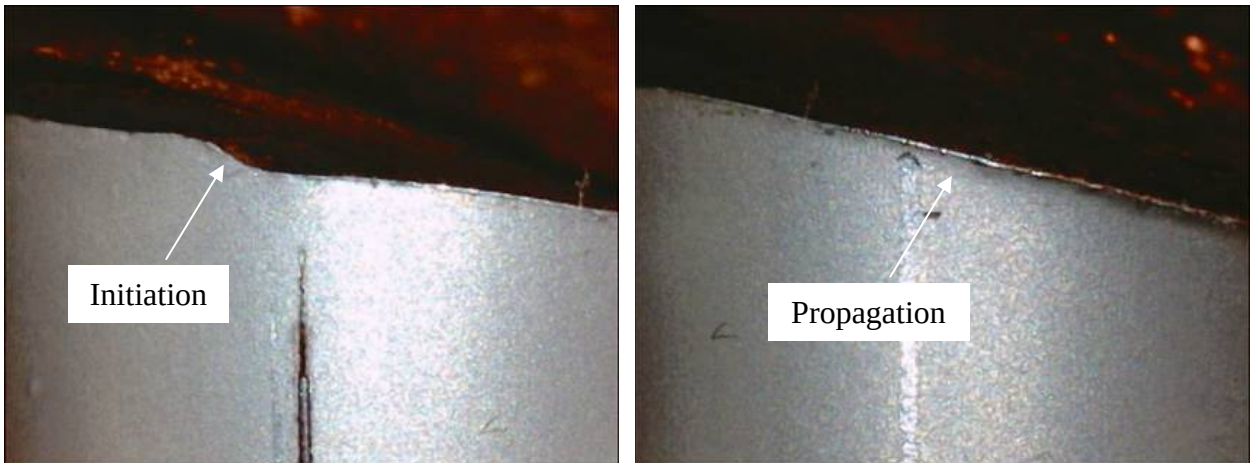

Figure 19. Crack initiation and propagation planes in Specimen 03-610: Box-2 path.

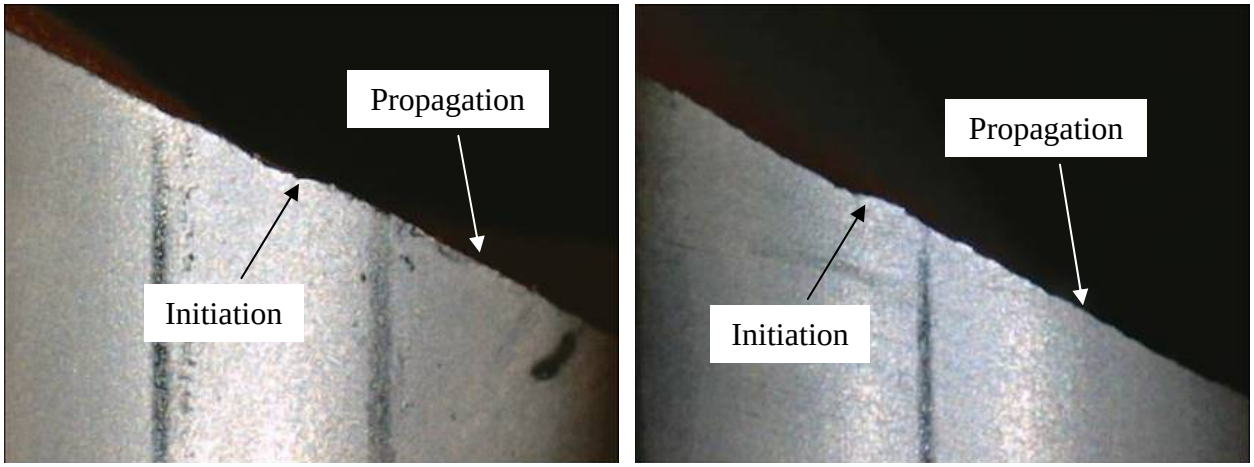

Figure 20. Crack initiation and propagation planes in Specimens 03-612 (left) and 03-613 (right): Check-2 path.

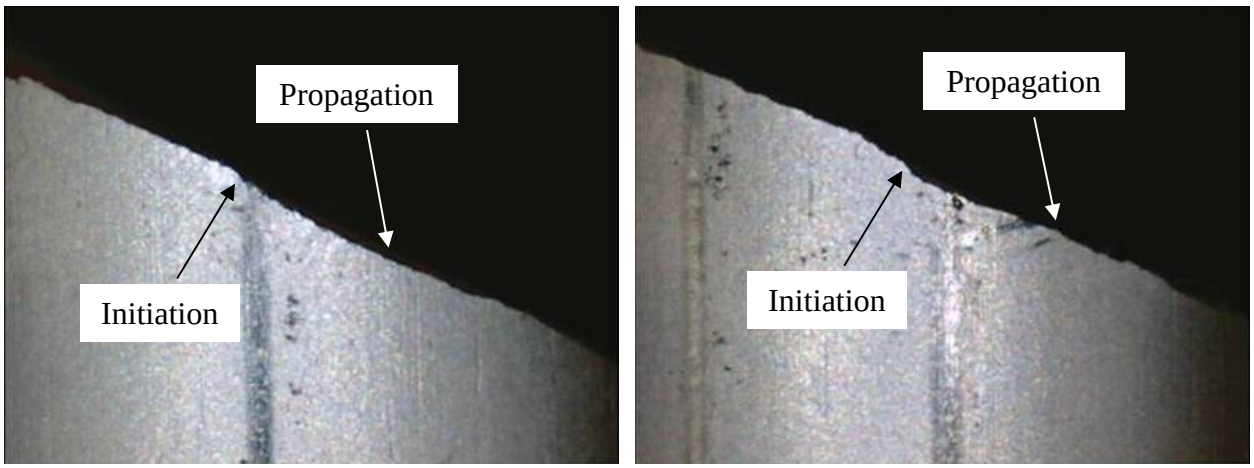

Figure 21. Crack initiation and propagation planes in Specimens 04-B00 (left) and 04-A97 (right): Proportional path.

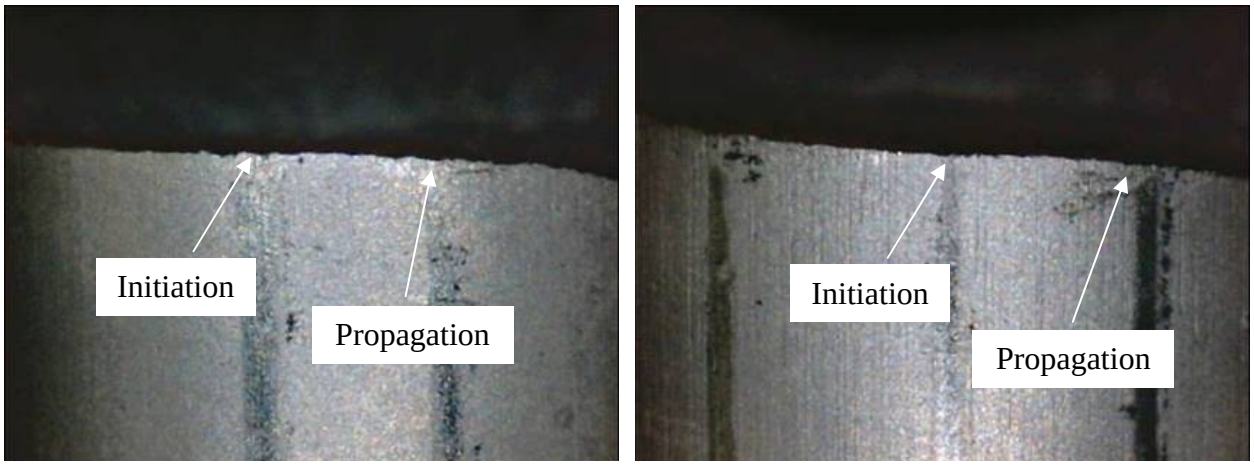

Figure 22. Crack initiation and propagation planes in Specimens 04-195 (left) and 04-A99 (right): Tor-Ax path.

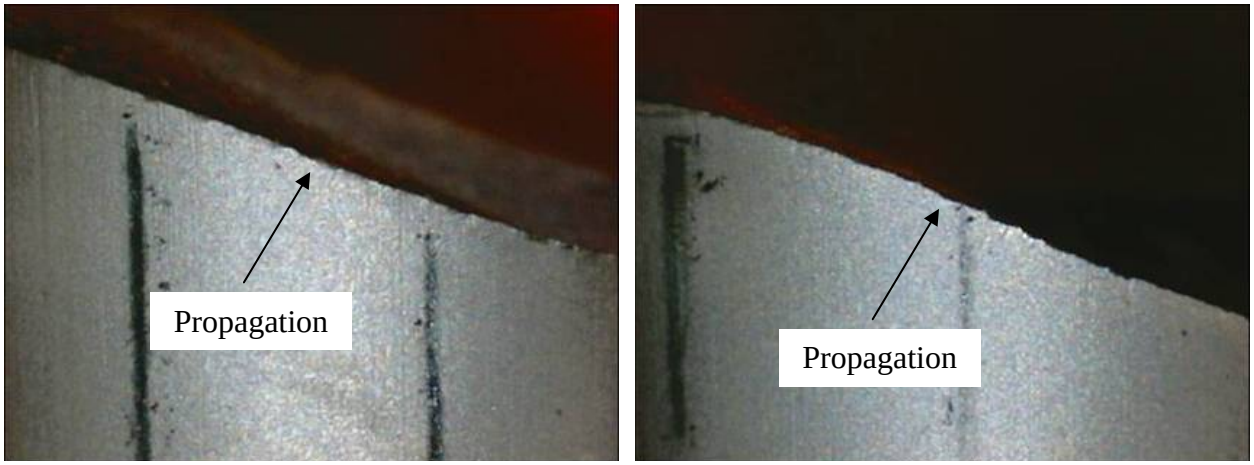

Figure 23. Crack propagation planes in Specimens 04-A93 (left) and 04-A95 (right): Tor-Pro path. Crack initiation planes were indiscernible.

Despite the difficulty in measuring the crack initiation planes, the results shown in Table 2 show relatively good agreement with the plane orientations predicted by Eq. (4). This provides further verification that this damage parameter accurately models the initiation of small cracks in Ti-6Al-4V under multiaxial loadings. It is also apparent that the measured crack propagation plane orientations are in very good agreement with the predicted values based on the Walker-type of parameter shown in Eq. (6), indicating that crack propagation was driven by the cyclic tensile stresses from the HCF cycles. Overall, the results shown in Table 2 appear to validate the hypothesis that the LCF cycles initiate cracks through shear mechanisms, and the HCF cycles then propagate these cracks to failure through tensile mechanisms.

Table 2
Plane Orientations for Crack Initiation and Propagation

History	Specimen ID	Initiation		Propagation	
		Measured	Predicted	Measured	Predicted
Box-2	03-609	17°	18°	13°	14°
	03-610	32°	18°	13°	14°
Check-2	03-612	5°	6°	28°	30°
	03-613	11°	6°	30°	30°
Proportional	04-B00	52°	58°	25°	22°
	04-A97	52°	58°	22°	22°
Tor-Ax	04-195	1°	4°	1°	0°
	04-A99	2°	4°	2°	0°
	04-A96	5°	4°	5°	0°
Tor-Pro	04-A93	--	4°	21°	24°
	04-A95	--	4°	24°	24°

Conclusions

This study was conducted to assess the level of LCF/HCF interactions in Ti-6Al-4V under multiaxial loading conditions. Several mission histories were constructed consisting of 1 LCF cycle coupled with 5 – 50 HCF cycles. The missions were designed to provide varying load paths, and hence stress conditions, between the LCF and HCF cycles. In most histories, the LCF lives were on the order of 10^4 cycles and the HCF lives were on the order of 10^8 cycles. Thus, based on a linear cumulative damage analysis, the HCF cycles would be expected to contribute very little damage to the mission histories.

The results of this study indicate that, in certain cases, a very strong, nonlinear interaction effect between LCF and HCF cycles occurs in Ti-6Al-4V, but the level of interaction depends on the load path. It was initially hypothesized that the interaction would be strongest when the critical LCF and HCF damage planes coincided, which assumed the damage from both the LCF and HCF cycles were attributable to common mechanisms. However, the experimental results were inconsistent with the trends predicted by this analysis, indicating the damage mechanisms were likely different between the LCF and HCF cycles.

A second critical plane analysis, formulated on the hypothesis that LCF cycles initiate damage through shear mechanisms and HCF cycles subsequently propagate that damage through tensile mechanisms, produced very good qualitative agreement with the experimental results. This analysis utilized a new damage parameter for the LCF cycles that was shown to provide good correlation with baseline uniaxial and multiaxial fatigue data for Ti-6Al-4V. This parameter assumes cyclic shear stresses are primarily responsible for the initiation of small cracks, but normal stresses on the critical plane provide a secondary effect by increasing or decreasing crack-face interaction. The damage from the HCF cycles was modeled using a Walker type of parameter defined by the normal stresses on a given plane, which assumes that the HCF damage is attributable to cyclic tensile stresses.

Through comparison of the experimental results with the damage plots from this analysis, it was shown that, in most cases, the magnitude of the LCF (mission) life reduction was roughly

proportional to the peak value of the HCF damage parameter, regardless of the relative orientations between the LCF and HCF critical planes. The one test which did not follow this trend likely experienced an "overload" effect from the LCF cycle during HCF crack growth, which caused crack growth retardation. Furthermore, experimental measurement of crack initiation and propagation plane orientations corresponded very well with the predicted orientations from the critical-plane analysis.

These results appear to strongly validate the hypothesis that the HCF cycles propagated the LCF induced damage in these mission histories. The reduction in mission lives due to the LCF/HCF interactions was, in many cases, quite severe, indicating these types of interactions must be recognized and accounted for in a comprehensive fatigue life analysis. In the absence of HCF cycles, the cracks initiated by the LCF cycles continue to grow on the LCF critical planes throughout the majority of the test duration, resulting in longer lives (in terms of LCF cycles) due to the lower-energy crack propagation mechanisms. However, in the presence of the smaller-amplitude but more numerous HCF cycles, the LCF initiated cracks may then be propagated more quickly by the cyclic HCF tensile stresses. This phenomenon was best illustrated by the testing of the Tor-Ax mission histories, in which the HCF cycles propagated the LCF initiated cracks on the same plane, resulting in very severe life reductions.

For these multiaxial mission tests, the use of the Palmgren-Miner linear damage rule is highly nonconservative and unable to predict the level of damage interaction. Furthermore, the non-proportional multiaxiality of the load paths appears to have exacerbated the damage interactions, as similar studies based on uniaxial loading conditions have not demonstrated such a high level of interaction. This indicates that the variation in load path between the LCF and HCF cycles may act as an additional catalyst to drive the damage mechanisms from shear to tensile at an earlier stage in crack development. As shown here, a multiaxial critical-plane analysis that accounts for different damage mechanisms is capable of qualitatively predicting the level of LCF/HCF interactions. However, a thorough quantitative analysis would require a combined crack initiation and propagation study to reliably predict the level of LCF/HCF interactions in general components.

References

1. Stephens, R.I., Dindinger, P.M., and Gunger, J.E., "Fatigue Damage Editing for Accelerated Durability Testing using Strain Range and SWT Parameter Criteria," *International Journal of Fatigue*, Vol. 19, 1997, pp. 599-606.
2. Yan, J.H., Zheng, X.L., and Zhao, K., "Experimental Investigation on the Small-Load-Omitting Criterion," International Journal of Fatigue, Vol. 23, 2001, pp. 403-415.
3. Fatemi, A. and Yang, L., "Cumulative Fatigue Damage and Life Prediction Theories: A Survey of the State of the Art for Homogeneous Materials," *International Journal of Fatigue*, Vol. 20, 1998, pp. 9-34.
4. Manson, S.S., and Halford, G.R., "Practical Implementation of the Double Linear Damage Rule and Damage Curve Approach for Treating Cumulative Fatigue Damage," *International Journal of Fracture*, Vol. 17, 1981, pp. 169-192.
5. Halford, G.R. and Manson, S.S., "Reexamination of Cumulative Fatigue Damage Laws," *Structure Integrity and Durability of Reusable Space Propulsion Systems*, NASA DP-2381, NASA, 1985, pp. 139-145

6. McGaw, M.A., "Approaches to Cumulative Damage Analysis," *Material Durability/Life Prediction Modeling: Materials for the 21st Century*, ASME PVP-Vol. 290, 1994, pp. 95-106.
7. Mayer, H., Ede, C. and Allison, J.E., "Influence of Cyclic Loads Below Endurance Limit or Threshold Stress Intensity on Fatigue Damage in Cast Aluminum Alloy 319-T7," *International Journal of Fatigue*, Vol. 27, 2005, pp. 129-141.
8. Goodin, E., Kallmeyer, A.R., and Kurath, P., "Cyclic Event Identification and Fatigue Damage Assessment for Multiaxial Mission Loadings," *Proceedings of the 8th National Turbine Engine High Cycle Fatigue Conference*, Monterey, CA, 2003.
9. Goodin, E., Kallmeyer, A.R., and Kurath, P., "Evaluation of Nonlinear Cumulative Damage Models for Assessing HCF/LCF Interactions in Multiaxial Loadings," *Proceedings of the 9th National Turbine Engine High Cycle Fatigue Conference*, Pinehurst, NC, 2004.
10. Findley, W.N., "Fatigue of Metals Under Combinations of Stresses," *ASME Transactions*, Vol. 79, 1957, pp. 1337-1348.
11. Erickson, M., Kallmeyer, A.R., Goodin, E., Torkelson, E., and Kurath, P., "An Evaluation of Multiaxial Fatigue Data from Ti-6Al-4V using a Critical Plane Methodology," to be presented at the *9th International Fatigue Congress*, Atlanta, Georgia, May 2006.
12. Dowling, N.E., *Mechanical Behavior of Materials: Engineering Methods for Deformation, Fracture, and Fatigue*, 2nd Ed., Prentice-Hall, Upper Saddle River, ND, 1998.

APPENDIX A

Mission History (LCF/HCF) Data and Results
Ti-6Al-4V, Room Temperature
Half-Life Stress-Strain Data

Cyclic stress-strain properties used in FEA

E (Msi)*	G (Msi)*	ν	σ_y (ksi)	K' (ksi)	n'
16.98	6.29	0.349	109.22	124	0.0149

*Note: E = 16.87 Msi and G = 6.25 Msi specified elsewhere

		Strains		**Stresses**					
		(controlled)		Pseudo-elastic (measured)		Elastic-plastic (FEA)			
Spec ID	Time point	ε (%)	γ (%)	σ (ksi)	τ (ksi)	σ (ksi)	τ (ksi)	Mission life	LCF life (avg)
142-7	1	0.3004	0.4135	46.29	27.39	51.01	26.02	19,470	68,721
Box-1	2	-0.3071	0.4148	-53.69	27.36	-52.15	26.11		
	3	-0.3055	-0.4175	-52.97	-26	-51.87	-26.28		
	4	0.3052	-0.4171	47.52	-25.61	51.82	-26.25		
	5	0.3004	0.4135			51.01	26.02		
	6	0.3	-0.11	45.96	-5.78	50.94	-6.92		
	7	0.3	0.399	46.62	26.56	50.94	25.11		
	8	0.3004	0.4135			51.01	26.02		
178-6	1	0.2999	0.4142	49.37	27.55	50.92	26.07	21,422	68,721
Box-1	2	-0.307	0.4136	-50.61	28.85	-52.13	26.03		
	3	-0.306	-0.4167	-50.48	-25.85	-51.96	-26.23		
	4	0.3051	-0.4163	50.25	-25.62	51.81	-26.20		
	5	0.2999	0.4142			50.92	26.07		
	6	0.301	-0.107	48.88	-5.49	51.11	-6.73		
	7	0.298	0.396	48.64	26.5	50.60	24.92		
	8	0.2999	0.4142			50.92	26.07		
142-1	1	0.301	0.4064	45.88	27.07	51.11	25.58	48,787	68,721
Box-1	2	-0.308	0.415	-53.99	27.15	-52.30	26.12		
	3	-0.3058	-0.4156	-52.99	-26.25	-51.92	-26.16		
	4	0.3061	-0.4183	47.39	-25.68	51.98	-26.33		
	5	0.301	0.4064			51.11	25.58		
	6	0.302	-0.107	46.54	-5.82	51.11	-6.73		
	7	0.301	0.399	45.86	26.39	51.28	25.11		
	8	0.301	0.4064			51.11	25.58		
178-9	1	0.301	0.414	46.47	27.04	51.11	26.06	39,480	68,721
Box-1	2	-0.308	0.414	-54.43	26.79	-52.30	26.06		
	3	-0.305	-0.417	-53.59	-26.68	-51.79	-26.24		
	4	0.306	-0.416	47.75	-26.17	51.96	-26.18		
	5	0.301	0.414			51.11	26.06		
	6	0.302	-0.106	46.96	-6.14	50.94	-6.67		
	7	0.3	0.4	46.29	26.17	51.28	25.17		
	8	0.301	0.414			51.11	26.06		
03-609	1	0.31	0.417	48.35	28.10	52.64	26.23	9,815	68,721
Box-2	2	-0.309	0.411	-52.86	27.97	-52.47	25.85		
	3	-0.301	-0.429	-51.84	-26.26	-51.11	-26.98		
	4	0.311	-0.412	49.51	-25.01	52.81	-25.91		
	5	0.31	0.417			52.64	26.23		
	6	-0.0707	0.41	-12.90	27.90	-12.00	25.79		
	7	0.2953	0.41	47.37	27.90	50.14	25.79		
	8	0.31	0.417			52.64	26.23		
03-611	1	0.304	0.419	46.68	27.34	51.62	26.36	10,248	68,721
Box-2	2	-0.308	0.412	-54.19	26.78	-52.30	25.91		
	3	-0.301	-0.426	-52.24	-26.76	-51.11	-26.80		
	4	0.308	-0.412	48.07	-25.56	52.30	-25.91		
	5	0.304	0.419			51.62	26.36		
	6	-0.0806	0.41	-16.36	26.82	-13.69	25.79		
	7	0.306	0.41	46.94	26.82	51.96	25.79		
	8	0.304	0.419			51.62	26.36		

03-610	1	0.301	0.41	46.28	28.10	51.11	25.79	12,719	68,721
Box-2	2	-0.309	0.41	-55.30	27.58	-52.47	25.79		
	3	-0.301	-0.403	-52.66	-26.63	-51.11	-25.35		
	4	0.31	-0.412	52.57	-25.18	52.64	-25.91		
	5	0.301	0.41			51.11	25.79		
	6	-0.066	0.41	-14.53	27.87	-11.21	25.79		
	7	0.291	0.41	44.57	27.87	49.41	25.79		
	8	0.301	0.41			51.11	25.79		
178-4	1	0.0095	0.0084	-1.01	-7.28	-3.16	-12.07	44,544	43,744
Check-1	2	0.2977	0.8244	44.66	44.50	45.78	38.79		
	3	0.153	1.2162	19.26	69.58	21.21	63.21		
	4	0.277	0.853	41.16	48.74	42.27	40.57		
	5	0.153	1.21	19.47	68.48	21.21	62.82		
	6	0.2977	0.8244	44.66	44.50	45.78	38.79		
	7	0.0095	0.0084	-1.01	-7.28	-3.16	-12.07		
142-3	1	0.0045	0.0083	-1.84	-6.71	-3.94	-12.01	49,776	43,744
Check-1	2	0.299	0.814	41.42	44.95	46.07	38.20		
	3	0.153	1.2032	14.80	70.32	21.28	63.19		
	4	0.2776	0.8634	37.51	48.83	42.50	41.81		
	5	0.151	1.1893	14.56	69.68	20.94	62.32		
	6	0.299	0.814	41.42	44.95	46.07	38.20		
	7	0.0045	0.0083	-1.84	-6.71	-3.94	-12.01		
03-613	1	0.0000	0.0000	-2.00	-3.73	-3.26	-12.21	8,640	43,744
Check-2	2	0.3030	0.8340	46.48	49.71	45.75	38.48		
	3	0.1490	1.2300	20.35	75.17	21.04	63.24		
	4	0.3010	0.8190	46.05	49.19	45.75	38.48		
	5	0.0827	0.2240	11.44	10.81	8.68	1.05		
	6	0.2970	0.8040	45.62	48.11	45.07	37.53		
	7	0.0000	0.0000	-2.00	-3.73	-3.26	-12.21		
03-612	1	0.0000	0.0000	-1.18	-2.80	-3.26	-12.21	5,860	43,744
Check-2	2	0.3030	0.8320	46.91	50.74	45.75	38.48		
	3	0.1490	1.2300	20.74	76.47	21.04	63.24		
	4	0.3000	0.8240	46.43	50.71	45.75	38.48		
	5	0.0828	0.2354	12.19	12.69	8.87	1.46		
	6	0.2970	0.7980	46.07	48.82	45.24	36.85		
	7	0.0000	0.0000	-1.18	-2.80	-3.26	-12.21		
04-A94	1	0.0491	0.0535	9.33	3.36	8.34	3.37	15,712	74,217
Prop	2	0.4596	0.6240	77.68	39.37	78.04	39.25		
	3	0.0497	0.0569	9.47	3.55	8.44	3.58		
	4	0.3599	0.4876	61.28	30.90	61.11	30.67		
04-B00	1	0.0484	0.0521	3.09	4.63	8.22	3.28	56,324	74,217
Prop	2	0.4579	0.6255	72.18	40.92	77.75	39.34		
	3	0.0521	0.0585	3.47	5.02	8.85	3.68		
	4	0.3611	0.4914	55.58	32.42	61.31	30.91		
04-A97	1	0.0481	0.0546	9.49	3.19	8.17	3.43	53,132	74,217
Prop	2	0.4620	0.6290	79.00	39.19	78.45	39.56		
	3	0.0495	0.0538	8.11	2.99	8.40	3.38		
	4	0.3614	0.4937	61.23	30.54	61.37	31.05		
04-195	1	0.0934	0.6870	14.26	45.51	15.86	43.21	3,408	72,926
Tor-Ax 1	2	0.0934	-0.691	14.26	-43.14	15.86	-43.46		
	3	0.4755	0.0000	76.69	0.00	80.74	0.00		
	4	0.0934	0.0000	14.27	0.00	15.86	0.00		
04-A99	1	0.0922	0.6843	14.33	44.11	15.66	43.04	3,968	72,926
Tor-Ax 1	2	0.0922	-0.6910	14.33	-44.57	15.66	-43.47		
	3	0.4742	0.0000	76.65	0.00	80.52	0.00		
	4	0.0922	0.0000	14.33	0.00	15.66	0.00		
04-A96	1	0.09306	0.6824	14.35	44.50	15.80	42.92	6,470	72,926
Tor-Ax 2	2	0.09306	-0.6904	14.35	-44.18	15.80	-43.43		
	3	0.3884	0.0000	63.02	0.00	65.95	0.00		
	4	0.0931	0.0000	14.35	0.00	15.80	0.00		
04-A93	1	0.0910	0.6940	10.06	43.35	15.45	43.65	3,072	72,926
Tor-Pro	2	0.0930	-0.7110	10.55	-46.08	15.79	-44.72		
	3	0.3952	0.5042	59.56	31.19	67.10	31.71		
	4	0.0892	0.0106	9.69	-0.23	15.15	0.67		
04-A95	1	0.0933	0.6930	13.28	44.06	15.84	43.59	2,816	72,926
Tor-Pro	2	0.0928	-0.7130	13.12	-45.82	15.76	-44.85		
	3	0.3954	0.5040	62.38	32.21	67.14	31.70		
	4	0.0898	0.0106	11.96	0.43	15.25	0.67		